International Journal of
Science and Engineering Investigations vol. 4, issue 41, June 2015
ISSN: 2251-8843

Design and Development of a Novel Bistatic DIAL Measurement System for Aviation Pollutant Concentrations

Alessandro Gardi[1], Roberto Sabatini[2]
[1,2]School of Aerospace, Mechanical and Manufacturing Engineering, RMIT University, Melbourne, VIC 3000, Australia
([2]roberto.sabatini@rmit.edu.au)

Abstract-This paper presents the research activities aimed at developing a flexible and low-cost measurement system for the determination of aviation-related pollutant concentrations in the vicinity of airports and other dense air traffic contexts. The proposed bistatic Light Detection and Ranging (LIDAR) system consists of two non-collocated components. The source component consists of a tuneable laser emitter, which can either be installed on a Remotely Piloted Aircraft System (RPAS) or operated from fixed and movable surface installations. The sensor component is constituted by a target surface calibrated for reflectance and a rail-mounted visible or infrared camera calibrated for radiance. The system performs Differential Absorption LIDAR (DIAL) measurements. The relevant opportunities and challenges, and the viability of the system in the intended operational environments are discussed. Numerical simulation results show promising performances in term of error expected error budget even in degraded meteorological conditions, which are comparable to the more complex and relatively costly monostatic LIDAR techniques currently available.

Keywords-*Aircraft Emissions, Differential Absorption, LIDAR, Pollutant Measurement, Sustainable Aviation*

I. INTRODUCTION

The steady growth of air transport at the global scale in the last decades has prompted social, political and scientific reactions to address its largely unsustainable evolution. Although aviation is currently producing less than 3% of the overall man-made CO_2 emissions, the global community is working to reduce the relative level of emissions as growth in air transport is forecast to increase such emissions by 50% over current levels by 2050 [1]. Major research and development programmes were therefore launched, including Clean Sky, NextGen, SESAR, Greener by Design, Environmentally Responsible Aviation, and are now delivering their preliminary outcomes to the industry and to the political decision-makers. The R&D activities are focusing on several concepts and technologies to reduce environmental impacts of flight operations, as well as in manufacturing, logistics, assembly, and disposal chains. Fossil fuels are particularly addressed since at present they represent by far the largest energy source for aircraft propulsion. The combustion of fossil fuels originates a number of noxious compounds as well as greenhouse gases, of which carbon dioxide (CO_2) is the principal representative, being the largest component of exhaust emissions. As a reference, each ton of typical Jet-A1 fuel can develop up to 3.15 tons of CO_2 and therefore the impact of each single commercial flight, consuming several tons of fuel, is substantial. The legislation currently in place for noise pollution control and charging is gradually being extended to CO_2 and it is envisaged that will similarly involve other polluting gases as well in the future. Therefore, high air traffic density areas will likely be monitored in terms of pollutant emissions. Ignoring dedicated test-bench installations, the currently adopted measurement strategies for aircraft pollutant emission figures are based on the following techniques [2]:

- In-situ sampling by air quality stations: they are located in the vicinity of larger airports and are the main source for their average pollution figures. Their measurement is substantially affected by the aerodynamic advection and diffusion of pollutants and is therefore noticeably averaged in time and space. Additionally, all pollutant emissions from man-made and biogenic activities in the surroundings of the air quality station are detected and cumulatively participate to the measure. For all these reasons these measurements are natively incapable of discerning a single aircraft, let alone a particular phase of its flight.
- Indirect estimation exploiting on-board thermomechanical sensors: they are installed within the aircraft engines and more generally on board aircraft, allowing an indirect estimation of pollutant emissions based on certain models and assumptions. Most commonly installed sensors are typically measuring Fuel Flow (FF), Turbine Entry Temperature (TET), Exhaust Gas Temperature (EGT), Engine Pressure Ratio (EPR), engine rotation speed (N_1, N_2, N_F...) and acoustic vibrations. The indirect estimation of pollutant emissions is analytically or heuristically derived from these thermodynamic and mechanical measurements, and is based on nominal conditions. Significantly off-design or degraded conditions of engine, fuel chemical composition, fuel transport or fuel storage conditions may violate key assumptions and hence affect the validity of such indirect measurements.

- Remote sensing by satellites, aircraft and balloons: The most widely used techniques for remote atmospheric sounding are based on absorption spectroscopy performed by passive electro-optic systems and on differential absorption measurements performed by LIDAR. A number of airborne and spaceborne laser systems have been adopted for large-scale CO_2 column density measurement campaigns [3-8]. Remote sensing from satellites and conventional aircraft are nonetheless affected by substantial costs and a rather limited flexibility in terms of space and time patterns and resolutions of the measures.

Current research activities are addressing new sensor technologies and measurement techniques for the determination of aviation pollutant concentrations. The new systems should feature either: greater operational flexibility, better sensitivity, accuracy, precision, reliability, greater spectral/ spatial/ temporal resolutions, and reduced weight/ volume/ costs. The research community is interested, in particular, in the spatial and temporal variations of macroscopic observables, and on the microphysical and chemical properties of atmospheric constituents and pollutants, including molecular, aerosol and particulate species [9-11]. An accurate measurement of CO_2 concentration variations in space and time related to aircraft operations is particularly important. The advent of powerful LIDAR systems with low weight and packaged in relatively small casings, makes them ideally suited for measuring the column densities of various important molecular species, including carbon oxides (CO_X), nitrogen oxides (NO_X), sulphur dioxides (SO_X), O_2 and ozone (O_3), both locally and over extended geographic areas [12, 13]. The Near-Infrared (NIR) region of the atmospheric propagation spectrum is dominated by molecular absorption from H_2O, CO and CO_2. A comparison with recorded spectra enables the identification of relatively strong and isolated CO and CO_2 transitions for unambiguous species detection [14]. These transitions have formed the basis of NIR sensors for measurements of CO and CO_2 mole fractions in exhaust gases using extraction-sampling techniques and for non-intrusive measurements of CO_2 in high-temperature combustion environments. Based on the demonstrated potential of Differential Absorption LIDAR (DIAL) [15-17], new airborne DIAL systems will greatly benefit from the technological advances in tuneable, compact and low-cost laser emitters enabling further portions of the spectrum to be exploited for multi-species pollutant concentration measurements.

II. Conceptual Design

The bistatic measurement system was conceptually presented in [2, 18], based on previous research [8, 10, 11, 19-22]. As depicted in Fig. 1, the proposed system consists of a LIDAR emitter installed on a Remotely Piloted Aircraft System (RPAS) or on fixed/movable surface installations, and a sensor component.

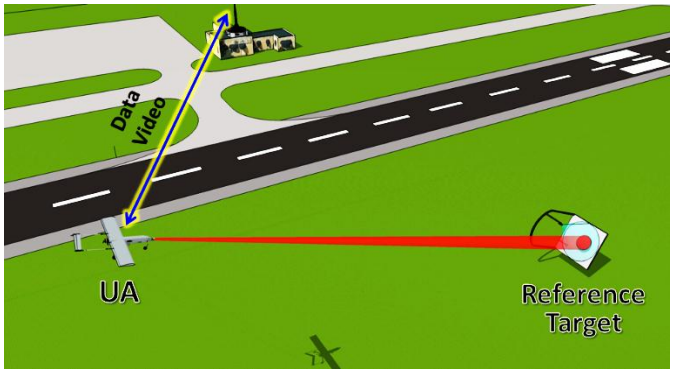

Figure 1. Representation of the bistatic DIAL system (not to scale)

The sensor component consists of a target surface featuring high and diffused reflectance and exhibiting Lambertian behaviour, such as Spectralon™, and a visible/infrared camera mounted on a rail. The RPAS platform flies pre-determined trajectories based on the required space and time frames of the measurement. Fig. 2 depicts the payload bay of a recent variant of the AEROSONDE RPAS, which will serve as the initial reference for the system components design.

Figure 2. Payload bay of a recent variant of the AEROSONDE RPAS

In [2] we introduced the key features of the measuring system and discussed the rationale supporting its development. A calibration technique was also introduced, employing a second ground-based LIDAR emitter and electro-optics photo-detectors. This paper reviews and updates our research results with an identification of operational and technical requirements for a first experimental prototype system to be employed on a suitable RPAS platform. The proposed system is based on the DIAL technique. The laser source emits beams at two predefined wavelengths. The first wavelength (λ_{ON}) is selected in correspondence of a major vibrational band of the targeted pollutant molecule (on-absorption line), clear from the transition/vibration spectrum of other atmospheric components. The second wavelength (λ_{OFF}) is selected in proximity of the first, but outside the vibrational band (off-absorption line) of the targeted pollutant species, so that the difference in cross-sections, $\Delta\psi \triangleq \psi(\lambda_{ON}) - \psi(\lambda_{OFF})$ is maximised. A number of databases and atmospheric Radiative Transfer Model (RTM) codes are available and allow an accurate estimation of the

propagation spectrum for identifying the optimal combination of DIAL wavelengths based on the mentioned criteria. The functional block diagram of the bistatic DIAL measurement system is represented in Fig. 3.

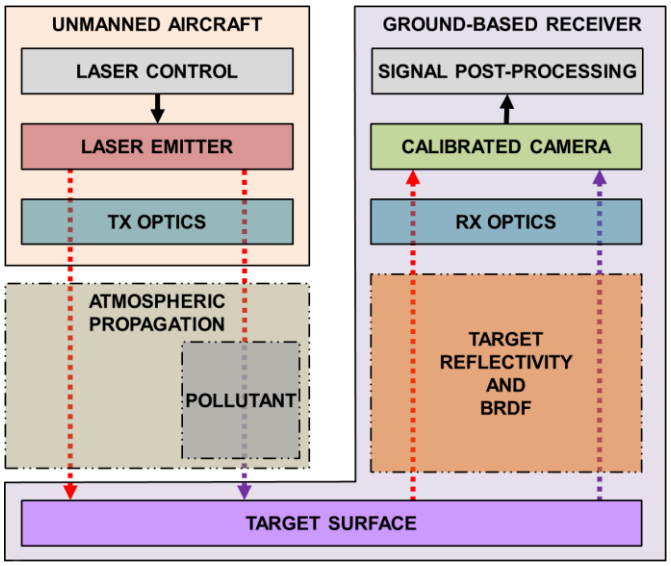

Figure 3. Functional block diagram of the bistatic DIAL measurement system

III. Atmospheric Laser Beam Propagation

The propagation of laser radiation in atmosphere is affected by a number of linear and nonlinear effects. In [18] we described the following expression for the peak irradiance I_P, accounting for absorption, scattering, diffraction, jitter, atmospheric turbulence and thermal blooming effects assuming a Gaussian profile of the laser beam at the source and an average focused irradiance [23, 24]:

$$I_P(z,\lambda) = \frac{b(z)\,\tau(z,\lambda)\,P(\lambda)}{\pi\left(a_d^2(z,\lambda) + a_j^2(z) + a_t^2(z,\lambda)\right)} \quad (1)$$

where z is the linear coordinate along the beam, λ is the wavelength, $P(\lambda)$ is the transmitted laser power, b is the blooming factor, $\tau(z,\lambda)$ is the transmittance coefficient, which accounts for absorption and scattering associated with all molecular and aerosol species present in the path. The 1/e beam radiuses associated with diffraction, $a_d(z,\lambda)$, beam jitter, $a_j(z)$, and turbulence, $a_t(z,\lambda)$, can be calculated as [11, 23]:

$$a_d(z,\lambda) = \frac{Qz\lambda}{2\pi a_0} \quad (2)$$

$$a_j^2(z) = 2\langle\Theta_x^2\rangle\, z^2 \quad (3)$$

$$a_t(z,\lambda) = \frac{2\,C_N^{6/5} z^{8/5}}{\lambda^{1/5}} \quad (4)$$

where Q is the beam quality factor, a_o is the beam *1/e* radius, $\langle\Theta_x^2\rangle$ is the variance of the single axis jitter angle that is assumed to be equal to $\langle\Theta_y^2\rangle$, and C_N^2 is the refractive index structure constant. An empirical model for the blooming factor $b(z)$, which is the ratio of the bloomed I_B to unbloomed I_{UB} peak irradiance, is:

$$b(z) = \frac{I_B}{I_{UB}} = \frac{1}{1 + 0.0625\,N^2(z)} \quad (5)$$

N is the thermal distortion parameter, calculated as:

$$N(z) = \frac{-n_T\,\alpha_m\,P\,z^2}{\pi\,d_0\,v_0\,c_P\,a_0^3} \cdot \left[\frac{2}{z^2}\int_0^R \frac{a_0}{a(z')}dz' \int_0^{z'} \frac{a_0^2\,v_0\,\tau''}{a}\,dz''\right] \quad (6)$$

where v_o is the uniform wind velocity in the weak attenuation limit ($\gamma z << 1$), n_T, d_o, and c_p are, respectively, the coefficients of index change with respect to temperature, density, and specific heat at constant pressure. The transmittance coefficient τ depends on the integral effect of absorption and scattering phenomena, both for molecular and aerosol species, on the entire beam length. The expression of Beer's law highlighting such dependences can therefore be written as:

$$\tau(z,\lambda) = e^{-\int_0^z \gamma(z,\lambda)\,dz} = e^{-\int_0^z [\alpha_m(z,\lambda) + \alpha_a(z,\lambda) + \beta_m(z,\lambda) + \beta_a(z,\lambda)]\,dz} \quad (7)$$

Where α are the absorption coefficients and β are the scattering coefficients, the subscripts *m* and *a* refer respectively to molecular and aerosol contributions. When referring to the integral absorption and scattering due to specific molecular species, it is more appropriate to express the transmittance with the following model:

$$\tau(z,\lambda) = e^{-\int_0^z \gamma(z,\lambda)\,dz} = e^{-\int_0^z \sum_i [\psi_i(\lambda)\cdot n_i(z)]\,dz} \quad (8)$$

where:

$\psi_i(\lambda)$ = cross-section of the i[th] species

n_i = molecular volume density of the i[th] species

From Eq. 8, the fraction between the measured incident laser energy associated with the on-absorption line of pollutant species P and the one associated with the off-absorption line, $R_{ON/OFF}$, can be expressed as [2]:

$$R_{\frac{ON}{OFF}} = \frac{E(\lambda_{ON})}{E(\lambda_{OFF})} = \frac{\tau_{ON}}{\tau_{OFF}} = e^{-[\psi_P(\lambda_{ON}) - \psi_P(\lambda_{OFF})]\int_0^D n_P(r)\,dr} \quad (9)$$

where D is the total beam length. The total pollutant column density N_P, which is the integral of the molecular volume density on the entire beam, is therefore:

$$N_P = \int_0^D n_P(r)\,dr = \frac{-\ln(R_{ON/OFF})}{\Delta\psi} \quad (10)$$

The average molecular volume concentration of the pollutant on the path, $\tilde{n}_P$, is therefore:

$$\tilde{n}_P = \frac{N_P}{D} = \frac{-\ln(R_{ON/OFF})}{D \cdot \Delta\psi} \quad (11)$$

As evident from Eq. 9 to 11, the bistatic DIAL measurement system neglects most of the parasite phenomena such as atmospheric visibility, particulate, rain and other precipitations, which would have elsewhere introduced a number of additional uncertainties in the system. The parasite effects, in fact, are assumed to equally affect the off-absorption and the on-absorption transmittances. For the specific carbon dioxide (CO_2) measurement system implementation, a successfully adopted on-absorption wavelength is the centre-line of R-branch at $\lambda_{ON} = 1572.335\ nm$ [3-7, 25, 26], in the Near-InfraRed (NIR). The SO_2 exhibits prominent spectral resonance in the Ultra-Violet (UV) range, and, in particular, in the region of 280 to 310nm, although infrared spectral features are also known, and in particular between 3970 and 4030 nm.

IV. Particle Retrieval

The retrieval of aerosol concentrations was originally examined in [10]. As per eq. 7, both molecular and aerosol concentrations in the transmission medium (i.e. the atmosphere) introduce absorption and scattering phenomena that affect the laser beam propagation. Therefore, the atmospheric transmittance measurement data accumulated in a certain time period using passive imaging systems enable the retrieval of aerosol concentrations as well. The difficulty in developing inversion algorithms lies in the fact that the input optical data are related to the investigated microphysical parameters through nonlinear integral equations of the first kind (Fredholm equations), which cannot be solved analytically. The generalised form of the Fredholm equation for atmospheric data retrieval is:

$$\alpha(\lambda), \beta(\lambda) = \int K_{\alpha,\beta}(r, n, k, \lambda) \cdot D(r) dr \quad (12)$$

where $\alpha(\lambda)$, and $\beta(\lambda)$ represent the optical data, $K_{\alpha,\beta}$ is the atmospheric kernel function (containing information on particle size, refractive index etc.) and $D(r)$ is the particle size distribution. The numerical solution of these equations leads to the so called ill-posed inverse problem. Such problems are characterised by a strong sensitivity of the solution space toward uncertainties of the input data, the non-uniqueness of the solution space, and the incompleteness of the solution space. In fact, the solution space may still be correct in a mathematical sense, but might not necessarily reflect the physical conditions. As the problem cannot be entirely defined by the measurements, a priori knowledge of the state vector is required in order to determine the most probable solution, with a probabilistic Bayesian approach. Let $\boldsymbol{y}$ be the measurement vector containing the measured radiances, and $\boldsymbol{x}$ be the concentration of a given constituent, then the general remote sensing equation can be written as follows [13]:

$$\boldsymbol{y} = f(\boldsymbol{x}, \boldsymbol{b}) + \boldsymbol{\epsilon} \quad (13)$$

where f represents the forward transfer function, $\boldsymbol{b}$ the other parameters affecting the measurement, and $\boldsymbol{\epsilon}$ the measurement noise. In the case of instruments measuring laser radiance, the vector $\boldsymbol{b}$ includes the target surface reflectance and radiance features (BRDF, reflectivity, emissivity and temperature), the variables describing the atmospheric state (vertical turbulence profile, temperature, water vapour and other atmospheric constituents, clouds, aerosols, etc.), and some characteristics of the measurement instruments (spectral response functions and resolution). The inverse problem consists in retrieving $\hat{\boldsymbol{x}}$, an estimate of the true state $\boldsymbol{x}$, from the measurement $\boldsymbol{y}$, and can be expressed as:

$$\hat{\boldsymbol{x}} = R(\boldsymbol{y}, \hat{\boldsymbol{b}}) = R(f(\boldsymbol{x}, \boldsymbol{b}) + \boldsymbol{\epsilon}, \hat{\boldsymbol{b}}) \quad (14)$$

where $\hat{\boldsymbol{b}}$ is an estimate of the non-retrieved parameters $\boldsymbol{b}$, and R is the inverse transfer function. This a priori information consists of an a priori state vector $\boldsymbol{x_a}$ and its covariance matrix $\boldsymbol{S_a}$, which may be provided by model simulations. Therefore, the inverse problem can be rewritten as follows:

$$\hat{\boldsymbol{x}} = R(\boldsymbol{y}, \hat{\boldsymbol{b}}, \boldsymbol{x_a}) \quad (15)$$

Various inversion techniques were proposed. One of the most popular approaches is the inversion with regularisation, offering the advantage of reducing oscillations in the solution that are frequently experienced in data retrieved from electro-optical measurements [9, 23]. This approach consists in introducing constraints, such as derivative analysis (smoothness) of the particle size distribution functions, positive sign of the functions and maximum variations over time. The comprehensive inversion algorithm with regularisation is depicted in Fig. 4.

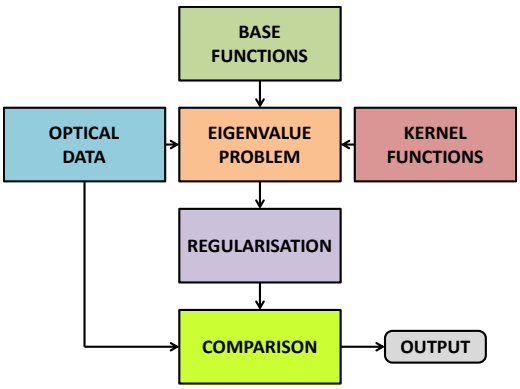

Figure 4. Block diagram of particle retrieval algorithm [10].

Using appropriate kernel/base functions, this algorithm can deliver parameters such as effective (average) particle radius, particle size distribution, total surface-area concentration, total number/volume concentrations, real and imaginary parts of the refractive index, single scattering albedo, etc. The base functions are Gaussian fits of the existing particle concentration data and are used to reconstruct the investigated particle size distributions. The kernel functions describe the

interaction of laser radiation with the atmosphere and contain information about the atmospheric transmittance, including scattering and absorption processes.

V. Model-Based Approach

Analytical expressions of the transmittances were developed for all the atmospheric windows in the infrared spectrum considering the parasite effects of atmospheric visibility, precipitation and fog [11]. By means of analytical inversion of the transmittance models, and thanks to an accurate sensing of local atmospheric conditions, it is also possible to determine the pollutant concentration without employing differential absorption measurements, by measuring the difference between the actually detected incident energy on the on-absorption line alone, and the model-based prediction for the off-absorption line. Although this technique simplifies the system architecture and potentially enable the adoption of less expensive non-tuneable laser emitters, the resulting error is heavily dependent on the quality and confidence of the measure of all parasite factors such as atmospheric visibility, temperature, pressure, humidity and precipitation. The theoretical model is based on comparison with the available extinction models for the i^{th} atmospheric window [24]. By introducing the total condensed water along the laser beam path, w, the meteorological visibility, V, and the rainfall rate R ,the empirically derived atmospheric transmittance values (off-absorption) for the 4th atmospheric window are summarised in Table 1 [24], where $k_{1,2...6}$ are correction factors experimentally determined as in [11]. The expressions of Table 1 are valid at mean sea level only. In order to extend the validity of the models, the dependency on altitude h Above Mean Sea Level (AMSL) shall be introduced. A number of empirical relationships for the altitude correction have been experimentally determined for NIR lasers depending on the grazing angles [11].

VI. Laboratory Calibration

The photo-camera calibration is an experimental procedure that allows determination of the Integrated Radiance Response Function (AIRF) [11, 21]. A highly selective filter (i.e., response centred on the laser wavelength) is used in conjunction with the photo-camera to detect the laser spot energy on the target and to generate a Pixel Intensity Matrix (PIM) in a high resolution greyscale format. The calibration setup is shown in Fig. 5.

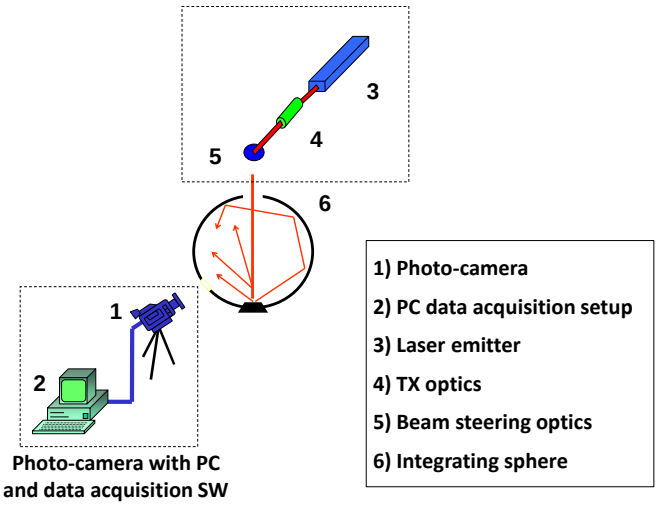

Figure 5. Layout of the photo-camera calibration.

TABLE I. Empirical expressions for the atmospheric off-absorption transmittance in the 4th atmospheric window.

CONDITION	EMPIRICAL MODEL
$V \geq 6\ km, \quad w \geq 1.1\ mm$	$\tau_{OFF}(z,w,V) \cong \mathrm{k}_1 \cdot 0.6432 \left(\frac{1.1}{w}\right)^{0.222} \cdot e^{-\frac{3.91}{V} z\, 0.3836^{-(0.0057V+1.025)}}$
$V < 6\ km, \quad w \geq 1.1\ mm$	$\tau_{OFF}(z,w,V) \cong \mathrm{k}_2 \cdot 0.6432 \left(\frac{1.1}{w}\right)^{0.222} \cdot e^{-\frac{3.91}{V} z\, 0.3836^{-0.585\sqrt[3]{V}}}$
$V \geq 6\ km, \quad w < 1.1\ mm$	$\tau_{OFF}(z,w,V) \cong \mathrm{k}_3 \cdot e^{-0.422\sqrt{w}-\frac{3.91}{V} z\, 0.3836^{-(0.0057V+1.025)}}$
$V < 6\ km, \quad w < 1.1\ mm$	$\tau_{OFF}(z,w,V) \cong \mathrm{k}_4 \cdot e^{-0.422\sqrt{w}-\frac{3.91}{V} z\, 0.3836^{-0.585\sqrt[3]{V}}}$
rain and $w \geq 1.1\ mm$	$\tau_{OFF}(z,w,R) \cong \mathrm{k}_5 \cdot e^{-0.422\sqrt{w}-0.365\ z\, R^{0.63}}$
rain and $w < 1.1\ mm$	$\tau_{OFF}(z,w,R) \cong \mathrm{k}_6 \cdot 0.6432 \left(\frac{1.1}{w}\right)^{0.222} \cdot e^{-0.365\ z\, R^{0.63}}$

The response of a single pixel in terms of Analogue Digital Unit (ADU) is:

$$ADU_{i,j} \propto \frac{A}{4 \cdot f_{\#}^2 + 1} \cdot g \cdot i_{time} \cdot \int_{\lambda_1}^{\lambda_2} (\tau_O \cdot \eta_D \cdot E_S)\, \mathrm{d}\lambda \quad (16)$$

where:

$\lambda_{1,2}$= limits of the photo-camera spectral band filter

η_D = detector quantum efficiency

E_S = spectral radiance

τ_0 = optics transmittance
A = pixel area
g = read-out electronics gain
$f_{\#}$ = optics f-number
i_{time} = photo-camera integration time

Therefore, the experimental parameters to be controlled during the calibration procedure are the integration time, the optics *f*-number and other settings of the photo-camera (e.g., the gain of the read-out electronics which may be selected by the operator). Fixing these parameters for a certain interval of integral radiance, it is possible to determine the AIRF of the camera by using an extended reference source. The function (calibration curve) so obtained is then used to determine the values of integral radiance for reconstructing the radiant intensity map of the target. Some mathematical models were developed and experimentally validated to calculate the optimal frame rate of the photo-camera [11]. In particular, photo-cameras are characterised by acquisition frequencies that typically are significantly different from the laser operating PRF. In the bistatic DIAL case, some additional consideration must be given to the alternated wavelengths of different pulses. A conceptual representation of the camera acquisition windows and dark zones in presence of laser pulses of alternating wavelength (different shades of red) is presented in Fig. 6. The parameters describing the train of pulses are the pulse duration (τ), the pulse period (T_P) and the PRF (f). Similarly, the camera image acquisition process is defined by the frame period (T_F) and the camera acquisition time (T_A). Generally T_A is inferior to T_F. The difference between T_F and T_A is the so called camera 'dark-time' (T_{dark}).

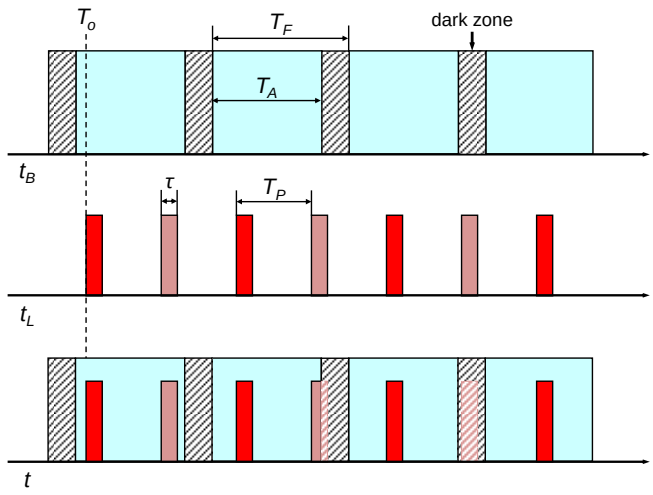

Figure 6. Photo-camera acquisition sequence and laser pulses.

Good synchronisation is extremely difficult even at low PRF and almost impossible as the PRF increases. Therefore a careful analysis is required in order to determine the optimal frame rate for the camera acquisition as a function of known laser pulse parameters. Since the camera frames are not synchronised with the laser pulses, considering the camera acquisition windows sequence as time base (t_B), the instant of arrival of the first laser pulse (reflected from the target) at the camera (T_o) can be treated as a random variable. Example results of a frame rate optimisation analysis, referred to laser emitters operating at f = 10 Hz and f = 40 kHz are summarised in Fig. 7, where P_{err} is the error probability.

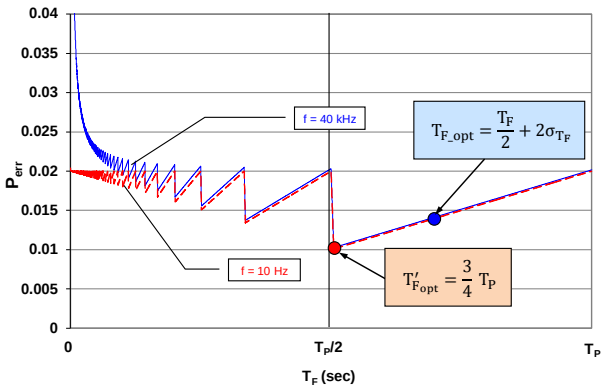

Figure 7. Results of NIR camera frame rate optimisation analysis.

VII. In-Situ Calibration Technique

In order to enable in-situ calibration of the bistatic LIDAR measurement we introduce a calibration system, represented in Fig. 8.

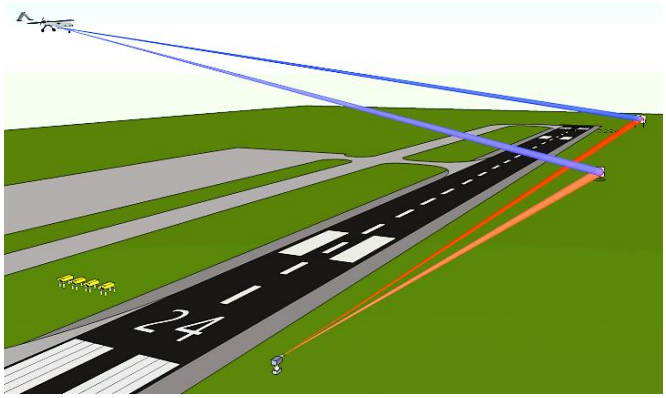

Figure 8. In-situ calibration layout.

In particular, an additional co-located NIR laser emitter and detector complex is installed on the ground at known distances from the first target surface and from an additional target surface, of equivalent specifications of the first, but without the NIR camera. The quality of the calibration is directly associated with the relative distance between the target surfaces, as evident from the following equations. As a reference, the assumed relative distances are, in particular, $\Delta d = d_2 - d_1 \geq 1\ km$. The anodic voltage at the receiver, V, can be expressed as [11]:

$$V = \mathrm{R_L} \cdot \mathrm{R_S} \cdot \mathrm{P}_R \tag{17}$$

where:
$\mathrm{R_L}$ = anodic load (Ω);
$\mathrm{R_S}$ = detector responsivity (A/W);
$\mathrm{P_R}$ = power reaching the detector (W);

By adopting two identical targets placed at different slant ranges, d_1 and d_2, at the same elevation above mean sea level (AMSL) at a similar bearing from the emitter/receiver, we can assume that the extinction coefficienton the off-absorption spectral line, γ_{OFF}, is constant between the two baselines. By detailing P_R, the following expressions can be written for the anodic voltages at the receiver, for the target surface 1, V_1, and 2, V_2:

$$V_1 = \mathrm{R_L} \cdot \mathrm{R_S} \cdot \left(P_B \cdot \rho \cdot \frac{e^{-2 \cdot \gamma \cdot d_1}}{d_1^2}\right) \tag{18}$$

$$V_2 = \mathrm{R_L} \cdot \mathrm{R_S} \cdot \left(P_B \cdot \rho \cdot \frac{e^{-2 \cdot \gamma \cdot d_2}}{d_2^2}\right) \tag{19}$$

where:

$\mathrm{P_B}$ = parameter accounting for the laser emitter power, for the window efficiencies and for the geometric characteristics of the beam;

ρ = target reflectivity.

The derived relation between the two sensed voltages is therefore:

$$\frac{V_1}{V_2} = \frac{P_{O1}}{P_{O2}} \cdot \frac{d_2^2}{d_1^2} \cdot e^{2 \cdot \gamma (d_2 - d_1)} \tag{20}$$

where $\mathrm{P_{O1,\,2}}$ is the transmitted laser powers (W).

The ground-level extinction coefficient relative to both spectral lines is therefore calculated as:

$$\gamma = \frac{1}{2\,\Delta d} \ln \left[\frac{\left(\frac{V_1}{P_{O1}}\right) d_1^2}{\left(\frac{V_2}{P_{O2}}\right) d_2^2} \right] \tag{21}$$

where $\Delta d = d_2 - d_1 \geq 1\ km$, as previously discussed.

The total uncertainty related to the extinction coefficient in eq. 9 is[11]:

$$\sigma_\gamma^2 = \frac{1}{(2\Delta \mathrm{d})^2} \cdot \left[\left(\frac{\sigma_{\mathrm{V1}}^2}{\mathrm{V}_1^2} + \frac{\sigma_{\mathrm{V2}}^2}{\mathrm{V}_2^2} \right) + \left(\frac{\sigma_{\mathrm{P_{O1}}}^2}{\mathrm{P}_{\mathrm{O1}}^2} + \frac{\sigma_{\mathrm{V_{O2}}}^2}{\mathrm{P}_{\mathrm{O2}}^2} \right) \right] + \frac{\gamma^2}{\Delta \mathrm{d}^2} \left[\left(\mathrm{d}_2 + \frac{1}{\gamma} \right)^2 \cdot \frac{\sigma_{\mathrm{d2}}^2}{\mathrm{d}_2} + \left(\mathrm{d}_1 + \frac{1}{\gamma} \right)^2 \cdot \frac{\sigma_{\mathrm{d1}}^2}{\mathrm{d}_1^2} \right] \tag{22}$$

By employing the same laser emitter for the ground and airborne systems we may assume constant errors in voltage and power, σ_V/V and σ_{Po}/P_O. Considering also the distance Δd several orders of magnitude higher than the extinction coefficient and rearranging the terms we obtain:

$$\sigma_\gamma = \frac{1}{\Delta\,\mathrm{d}} \sqrt{\frac{1}{2} \left(\frac{\sigma_{\mathrm{V}}^2}{\mathrm{V}^2} + \frac{\sigma_{\mathrm{P_O}}^2}{\mathrm{P}_{\mathrm{O}}^2} \right)} \tag{23}$$

In the calibration system design, it must be ensured that the overall uncertainty is an order of magnitude lower than the one associated with the bistatic LIDAR measurement system. From eq. 10, neglecting the uncertainty in $\Delta\psi$, the error on the pollutant column density measurement N_{CO_2} for the calibration system layout is:

$$\sigma_{CAL,N_{CO_2}} = \frac{1}{\Delta\psi} \cdot \sqrt{2[\sigma_\gamma^2 - cov(\gamma_{ON}, \gamma_{OFF})]} \tag{24}$$

By introducing the uncertainty in the extinction coefficient from (16), we finally obtain:

$$\sigma_{CAL,N_{CO_2}} = \frac{1}{\Delta\psi} \sqrt{\frac{1}{\Delta d} \left(\frac{\sigma_{\mathrm{V}}^2}{\mathrm{V}^2} + \frac{\sigma_{\mathrm{P_O}}^2}{\mathrm{P}_{\mathrm{O}}^2} \right) - 2 \cdot cov(\gamma_{ON}, \gamma_{OFF})} \tag{25}$$

This result clearly supports the selection of large relative distances between the targets, ideally in the range of 1~3 km or more if available. Similar distances are comparable to the typical runway lengths at major airports. Therefore, the calibration system may ideally be collocated parallel and in proximity of a runway, outside of the Instrument Landing System (ILS) sensitive areas where applicable.

VIII. Error Estimation

A preliminary error estimation was presented in [18]. The uncertainty associated with the measurement of the molecular volume concentration, derived from eq. 11, is:

$$\sigma_{\tilde{n}_P} = \frac{1}{D \cdot \Delta\psi} \sqrt{\left(\frac{\sigma_{R_{ON/OFF}}}{R_{ON/OFF}} \right)^2 + \left(\frac{\sigma_D \ln R_{ON/OFF}}{D} \right)^2 + \left(\frac{\sigma_{\Delta\psi} \ln R_{ON/OFF}}{\Delta\psi} \right)^2} \tag{26}$$

For a preliminary estimation, we introduced representative errors on the first two quadratic terms in eq. 16, specific to the bistatic DIAL implementation. Errors were introduced on the distance, σ_D, and on the differential energy measurement, which is translated into $\sigma_{R_{ON/OFF}}$ by means of the Bidirectional Reflectance Distribution Function (BRDF) of the target surface [11]. Assuming the operational conditions summarised in Table 2 and injecting source errors detailed in Table 3, the resulting relative error for the CO_2 volume density was calculated as $\frac{\sigma_{\tilde{n}_P}}{\tilde{n}_P}$ = 6.77 % [18]. These preliminary results, associated with the very low error figures from the monostatic Integral Path Differential Absorption (IPDA) LIDAR experimental campaigns [26] and with the estimated performance of the in-situ calibration technique, contribute to supporting the validity of the proposed bistatic DIAL measurement technique for high accuracy sensing of aviation-related pollutant concentrations. Experimental testing will be required to further corroborate these preliminary findings.

TABLE II. WORST-CASE OPERATIVE CONDITIONS [18].

Parameter	Value
Horizontal distance between the RPAS and the target surface	1000 m
RPAS Height Above Ground Level (AGL)	150 m
CO_2 volume density	300 ppm

TABLE III. ASSUMED SOURCE ERRORS [18].

Source	Magnitude	Affected Term	Error
Discrepancy in the incident angle between $E(\lambda_{ON})$ and $E(\lambda_{OFF})$	5° azimuth 5° elevation	$\frac{\sigma_{R_{ON/OFF}}}{R_{ON/OFF}}$	3.04 %
Degraded RPAS navigation performance	20 m horizontally 15 m vertically	$\frac{\sigma_D}{D}$	2.47%

IX. CONCLUSIONS AND FUTURE WORK

This paper reviewed the research activities focussing on the development of an innovative bistatic LIDAR system for the measurement of pollutant concentrations. The specific implementations for carbon dioxide (CO_2) and aerosol measurements were presented. The Differential Absorption LIDAR (DIAL) technique allows neglecting parasite effects such as atmospheric visibility, particulate and precipitation, and contributes to the overall accuracy and reliability of the proposed technique. The uncertainty analysis for CO_2 column density measurements showed that the proposed technique produces satisfactory results even in degraded meteorological conditions, which are comparable to the more complex and relatively costly monostatic LIDAR techniques currently available. Current research activities are investigating the extension of the system to other families of aviation pollutants such as nitrogen oxides (NO_X), sulphur oxides (SO_X), and Volatile Organic Compounds (VOC) taking advantage of the recent availability of tuneable laser emitters for multi-species detection. The research activities will involve laboratory testing as well as flight testing in various representative conditions. In particular, the development of the airborne component will benefit from the concurrent research activities on RPAS-based LIDAR systems [27-29]. The RPAS will be equipped with Differential GPS-based Time-and-Space-Position-Information (TSPI) systems that were developed for augmented navigation performance of both manned and unmanned aircraft [30, 31] in combination with integrity augmentation systems [32, 33]. The experimental flight testing activity will be performed in a suitably developed laser test range in full compliance with eye-safety requirements [11, 21, 34]. The full potential of the proposed bistatic DIAL measurement system will be exploited through its functional integration in the next generation of Air Traffic Management (ATM) systems [35, 36].

REFERENCES

[1] M. Janić, The sustainability of air transportation: a quantitative analysis and assessment, Ashgate Publishing, Ltd., 2007.

[2] A. Gardi, R. Sabatini, and G. Wild, "Unmanned aircraft bistatic lidar for CO_2 colum density determination", in proceedings of IEEE Metrology for Aerospace (MetroAeroSpace 2014), Benevento, Italy, 2014. DOI: 10.1109/MetroAeroSpace.2014.6865892

J. B. Abshire, H. Riris, G. R. Allan, C. J. Weaver, J. Mao, X. Sun, et al., "Pulsed airborne lidar measurements of atmospheric CO2 column absorption", Tellus, Series B: Chemical and Physical Meteorology, vol. 62, pp. 770-783, 2010. DOI: 10.1111/j.1600-0889.2010.00502.x

[3] M. A. Krainak, A. E. Andrews, G. R. Allan, J. F. Burris, H. Riris, X. Sun, et al., "Measurements of atmospheric CO2 over a horizontal path using a tunable-diode-laser and erbium-fiber-amplifier at 1572 nm", in proceedings of Conference on Lasers and Electro-Optics 2003 (CLEO '03), Baltimore, MD, USA, 2003, pp. 878 - 881

[4] H. Riris, J. B. Abshire, G. Allan, J. F. Burris, J. Chen, S. R. Kawa, et al., "A laser sounder for measuring atmospheric trace gases from space", in proceedings of SPIE 6750, Lidar Technologies, Techniques, and Measurements for Atmospheric Remote Sensing III, Florence, Italy, 2007. DOI: 10.1117/12.737607

[5] G. R. Allan, H. Riris, J. B. Abshire, X. Sun, E. Wilson, J. F. Burris, et al., "Laser sounder for active remote sensing measurements of CO_2 concentrations", in proceedings of IEEE/AIAA Aerospace Conference 2008 (AC2008), Big Sky, MT, USA, 2008, pp. 1-7. DOI: 10.1109/AERO.2008.4526387

[6] A. Amediek, A. Fix, G. Ehret, J. Caron, and Y. Durand, "Airborne lidar reflectance measurements at 1.57 μm in support of the A-SCOPE mission for atmospheric CO_2", Atmospheric Measurement Techniques Discussions, vol. 2, pp. 1487-1536, 2009

[7] R. Sabatini and M. A. Richardson, "Innovative methods for planetary atmospheric sounding by lasers", in proceedings of AIAA Space 2008 Conference, San Diego, CA, USA, 2008. DOI: 10.2514/6.2008-7670

[8] C. D. Rodgers, Inverse methods for atmospheric sounding: Theory and practice vol. 2, World scientific Singapore, 2000.

[9] R. Sabatini, M. A. Richardson, H. Jia, and D. Zammit-Mangion, "Airborne laser systems for atmospheric sounding in the near infrared", in proceedings of SPIE 8433, Laser Sources and Applications, Photonics Europe 2012, Brussels, Belgium, 2012. DOI: 10.1117/12.915718

[10] R. Sabatini and M. A. Richardson, Airborne Laser Systems Testing and Analysis, RTO AGARDograph AG-300 Vol. 26, Flight Test Instrumentation Series, Systems Concepts and Integration Panel (SCI-126), NATO Science and Technology Organization, 2010.

[11] I. Veselovskii, A. Kolgotin, V. Griaznov, D. Müller, K. Franke, and D. N. Whiteman, "Inversion of multiwavelength Raman lidar data for retrieval of bimodal aerosol size distribution", Applied Optics, vol. 43, pp. 1180-1195, 2004. DOI: 10.1029/2003JD003538

[12] D. Müller, F. Wagner, U. Wandinger, A. Ansmann, M. Wendisch, D. Althausen, et al., "Microphysical particle parameters from extinction and backscatter lidar data by inversion with regularization: Experiment", Applied Optics, vol. 39, pp. 1879-1892, 2000

[13] Z. Kuang, J. Margolis, G. Toon, D. Crisp, and Y. Yung, "Spaceborne measurements of atmospheric CO2 by high‐resolution NIR spectrometry of reflected sunlight: An introductory study", Geophysical Research Letters, vol. 29, pp. 11-1, 2002

[14] W. B. Grant and R. D. Hake Jr, "Calibrated remote measurements of SO2 and O3 using atmospheric backscatter", Journal of Applied Physics, vol. 46, pp. 3019-3023, 1975. DOI: 10.1063/1.321992

[15] W. B. Grant, R. D. Hake Jr, E. M. Liston, R. C. Robbins, and E. K. Proctor Jr, "Calibrated remote measurement of NO_2 using the differential-absorption backscatter technique", Applied Physics Letters, vol. 24, pp. 550-552, 1974. DOI: 10.1063/1.1655049

[16] R. M. Schotland, "Errors in the lidar measurement of atmospheric gases by differential absorption", Journal of Applied Meteorology, vol. 13, pp. 71-77, 1974

[17] A. Gardi, R. Sabatini, and S. Ramasamy, "Bistatic LIDAR System for the Characterisation of Aviation-Related Pollutant Column Densities",

Applied Mechanics and Materials, vol. 629, pp. 257-262, 2014. DOI: 10.4028/www.scientific.net/AMM.629.257

[18] R. Sabatini, "Tactical Laser Systems Performance Analysis in Various Weather Conditions", in RTO-MP-001 - E-O Propagation, Signature and System Performance under Adverse Meteorological Conditions Considering Out of Area Operations, pp. 29-1 to 29-13, NATO Research and Technology Organization (RTO), Naples, Italy, 1998.

[19] R. Sabatini, F. Guercio, and S. Vignola, "Airborne laser systems performance analysis and mission planning", in RTO-MP-046 - Advanced Mission Management and Systems Integration Technologies for Improved Tactical Operations, NATO Research and Technology Organization (RTO), Florence, Italy, 1999.

[20] R. Sabatini and M. A. Richardson, "A new approach to eye-safety analysis for airborne laser systems flight test and training operations", Optics and Laser Technology, vol. 35, pp. 191-198, 2003. DOI: 10.1016/S0030-3992(02)00171-8

[21] R. Sabatini and M. A. Richardson, "Airborne Laser Systems Testing, Safety Analysis, Modelling and Simulation", presented at the 21st Annual Symposium of the Society of Flight Test Engineers - European Chapter, Vergiate (VA), Italy, 2010.

[22] F. G. Gebhardt, "High Power Laser Propagation", Applied Optics, vol. 15, pp. 1479-1493, 1976

[23] R. Sabatini and M. A. Richardson, "Novel atmospheric extinction measurement techniques for aerospace laser system applications", Infrared Physics and Technology, vol. 56, pp. 30-50, 2013. DOI: 10.1016/j.infrared.2012.10.002

[24] J. B. Abshire, A. Ramanathan, H. Riris, J. Mao, G. R. Allan, W. E. Hasselbrack, et al., "Airborne measurements of CO_2 column concentration and range using a pulsed direct-detection IPDA lidar", Remote Sensing, vol. 6, pp. 443-469, 2013. DOI: 10.3390/rs6010443

[25] J. B. Abshire, H. Riris, C. J. Weaver, J. Mao, G. R. Allan, W. E. Hasselbrack, et al., "Airborne measurements of CO_2 column absorption and range using a pulsed direct-detection integrated path differential absorption lidar", Applied Optics, vol. 52, pp. 4446-4461, 2013. DOI: 10.1364/AO.52.004446

[26] R. Sabatini, A. Gardi, and M. A. Richardson, "LIDAR Obstacle Warning and Avoidance System for Unmanned Aircraft", International Journal of Mechanical, Aerospace, Industrial and Mechatronics Engineering, vol. 8, pp. 62-73, 2014

[27] R. Sabatini, A. Gardi, S. Ramasamy, and M. A. Richardson, "A Laser Obstacle Warning and Avoidance System for Manned and Unmanned Aircraft", in proceedings of IEEE Metrology for Aerospace (MetroAeroSpace 2014), Benevento, Italy, 2014, pp. 616-621. DOI: 10.1109/MetroAeroSpace.2014.6865998

[28] R. Sabatini, A. Gardi, and S. Ramasamy, "A Laser Obstacle Warning and Avoidance System for Unmanned Aircraft Sense-and-Avoid", Applied Mechanics and Materials, vol. 629, pp. 355-360, 2014. DOI: 10.4028/www.scientific.net/AMM.629.355

[29] R. Sabatini, "High Precision DGPS and DGPS/INS Positioning for Flight Testing", in RTO-MP-043 - 6th Saint Petersburg International Conference on Integrated Navigation Systems, pp. 18-1 to 18-17, NATO Research and Technology Organization (RTO), Saint Petersburg, Russia, 1999.

[30] R. Sabatini and G. B. Palmerini, Differential Global Positioning System (DGPS) for Flight Testing, RTO AGARDograph AG-160 Vol. 21, Flight Test Instrumentation Series, Systems Concepts and Integration Panel (SCI-135), NATO Science and Technology Organization, 2008.

[31] R. Sabatini, T. Moore, and C. Hill, "A new avionics-based GNSS integrity augmentation system: Part 1 - Fundamentals", Journal of Navigation, vol. 66, pp. 363-384, 2013. DOI: 10.1017/S0373463313000027

[32] R. Sabatini, T. Moore, and C. Hill, "A new avionics-based GNSS integrity augmentation system: Part 2 - Integrity flags", Journal of Navigation, vol. 66, pp. 501-522, 2013. DOI: 10.1017/S0373463313000143

[33] R. Sabatini, "Innovative Flight Test Instrumentation and Techniques for Airborne Laser Systems Performance Analysis and Mission Effectiveness Evaluation", in proceedings of IEEE Metrology for Aerospace (MetroAeroSpace 2014), Benevento, Italy, 2014, pp. 1-17. DOI: 10.1109/MetroAeroSpace.2014.6865886

[34] A. Gardi, R. Sabatini, S. Ramasamy, and K. de Ridder, "4-Dimensional Trajectory Negotiation and Validation System for the Next Generation Air Traffic Management", in proceedings of AIAA Guidance, Navigation, and Control Conference (GNC 2013), Boston, MA, USA, 2013. DOI: 10.2514/6.2013-4893

[35] A. Gardi, R. Sabatini, S. Ramasamy, and T. Kistan, "Real-Time Trajectory Optimisation Models for Next Generation Air Traffic Management Systems", Applied Mechanics and Materials, vol. 629, pp. 327-332, 2014. DOI: 10.4028/www.scientific.net/AMM.629.327.